Available online at www.sciencedirect.com
ScienceDirect
International Journal of Heat and Mass Transfer 51 (2008) 4517–4527
International Journal of HEAT and MASS TRANSFER
www.elsevier.com/locate/ijhmt

Velocity–vorticity formulation for 3D natural convection in an inclined enclosure by BEM

J. Ravnik *, L. Škerget, Z. Žunič

Faculty of Mechanical Engineering, University of Maribor, Smetanova 17, SI-2000 Maribor, Slovenia

Received 1 January 2007
Available online 2 April 2008

Abstract

A natural convection phenomenon is studied in cubic and parallelepipedal inclined enclosures. The simulation of coupled laminar viscous flow and heat transfer is performed using a novel algorithm based on a combination of single domain Boundary element method (BEM) and subdomain BEM. The algorithm solves the velocity–vorticity formulation of the incompressible Navier–Stokes equations coupled with the energy equation using the Boussinesq approximation. The subdomain BEM is used to solve the kinematics equation, the vorticity transport equation and the energy equation. The boundary vorticity values, which are needed as boundary conditions for the vorticity transport equation, are calculated by singe domain BEM solution of the kinematics equation. Simulation results are compared with benchmark results for a cubic inclined enclosure for Rayleigh number values $10^3 \leqslant Ra \leqslant 10^5$. The results for an inclined enclosure with width to height ratio 1:2 are also presented.

PACS: 47.11.+j; 44.25.+f

Keywords: Subdomain boundary element method; Velocity–vorticity formulation; Laminar viscous fluid flow; Natural convection; Inclined enclosure

1. Introduction

Over the last few decades buoyancy-driven flows have been widely investigated. Enclosures differentially heated on two opposite sides under different inclination angles with respect to gravity are usually the target of research. Natural convection in a parallelepipedal enclosure is present in many industrial applications, such as cooling of electronic circuitry, nuclear reactor insulation and ventilation of rooms.

Research of the natural convection phenomena started with the two dimensional approach and has been recently extended to three dimensions. A benchmark solution for two dimensional flow of an incompressible fluid in a square differentially heated enclosure was presented by Davies [1]. He used the stream function-vorticity formulation. Vierendeels et al. [2,3] used a multigrid method to obtain a solution of a compressible fluid in a square enclosure for Rayleigh numbers between $Ra = 10^2$ and $Ra = 10^7$. Škerget and Samec [4] confirmed these results using a compressible 2D boundary element method (BEM) formulation. Weisman et al. [5] studied the transition from steady to unsteady flow for compressible fluid in a 1:4 enclosure. They found that the transition occurs at $Ra \approx 2 \times 10^5$. Ingber [6] used the vorticity formulation to simulate flow in both square and 1:8 differentially heated enclosures. Tric et al. [7] studied natural convection in a 3D cubic enclosure using a pseudo-spectra Chebyshev algorithm based on the projection–diffusion method with spatial resolution supplied by polynomial expansions. Lo et al. [8] also studied a 3D cubic enclosure under five different inclinations $\vartheta = 0°, 15°, 30°, 45°, 60°$. They used a differential quadrature method to

* Corresponding author. Tel.: +386 2 220 7745; fax: +386 2 220 7990.
E-mail addresses: jure.ravnik@uni-mb.si (J. Ravnik), leo@uni-mb.si (L. Škerget), zoran.zunic@uni-mb.si (Z. Žunič).

0017-9310/$ - see front matter © 2008 Elsevier Ltd. All rights reserved.
doi:10.1016/j.ijheatmasstransfer.2008.01.018

solve the velocity–vorticity formulation of Navier–Stokes equations employing higher order polynomials to approximate differential operators.

Simulations as well as experiments of turbulent flow were also extensively investigated. Hsieh and Lien [9] considered numerical modelling of buoyancy-driven turbulent flows in enclosures using RANS approach. 2D DNS was performed by Xin and Le Quéré [10] for an enclosure with aspect ratio 4 up to Rayleigh number, based on the enclosure height, 10^{10} using expansions in series of Chebyshev polynomials. Ravnik et al. [11] confirmed these results using a 2D LES model based on combination of BEM and FEM using the classical Smagorinsky model with Van Driest damping. Peng and Davidson [12] performed a LES study of turbulent buoyant flow in a 1:1 enclosure at $Ra = 1.59 \times 10^9$ using a dynamic Smagorinsky model as well as the classical Smagorinsky model with Van Driest damping.

A wide variety of methods have been used to simulate the natural convection phenomena. In this work we are presenting a novel algorithm, which is able to simulate 3D laminar viscous flow coupled with heat transfer by solving the velocity–vorticity formulation of Navier–Stokes equations using BEM. The velocity–vorticity formulation is an alternative form of the Navier–Stokes equation, which does not include pressure. The unknown field functions are the velocity and vorticity. In an incompressible flow, both are divergence free. Daube [13] pointed out that the correct evaluation of boundary vorticity values is essential for conservation of mass. Thus, the main challenge of velocity–vorticity formulation lies in the determination of boundary vorticity values. Several different approaches have been proposed for the determination of vorticity on the boundary. Wong and Baker [14] used a second-order Taylor series to determine the boundary vorticity values explicitly. Daube [13] used an influence matrix technique to enforce both the continuity equation and the definition of the vorticity in the treatment of the 2D incompressible Navier–Stokes equations. Liu [15] recognised that the problem is even more severe when he extended it to three dimensions. Lo et al. [8] used the differential quadrature method. Škerget et al. [16] proposed the usage of single domain BEM to obtain a solution of the kinematics equation in tangential form for the unknown boundary vorticity values and used it in 2D. This work was extended into 3D using a linear interpolation by Žunič et al. and using quadratic interpolation by Ravnik et al. [17] for uncoupled flow problems. In this work, we will extend our method presented in Ravnik et al. [17] for coupled fluid flow – heat transfer problems.

We will use single domain BEM for determination of boundary vorticity. All other equations will be solved by subdomain BEM [18]. Subdomain BEM solution of a partial differential equation, unlike the single domain BEM, leads to a sparse system of linear equations. A sparse system enables fast algebraic operations and does not require a lot of storage. Other methods of improving the efficiency of single domain BEM were proposed as well, e.g. methods based on the expansion of the integral kernel [19], dual reciprocity method [20] or compression of single domain full matrices [21,11].

In the next section of the paper we describe the natural convection phenomena, in the third section we write the governing equations of coupled viscous flow and heat transfer and in the fourth section describe our BEM based numerical solution. In the fifth section we present the results of simulations.

2. Natural convection in an inclined enclosure

Consider an enclosure filled with fluid subjected to a temperature difference on two opposite walls, while the rest of the walls are adiabatic. The fluid next to the hot wall will be heated and due to its decrease of density buoyancy will carry it upwards. An inverse phenomenon will occur along the cold wall, the fluid there will be colder and denser and thus it will travel downwards. This phenomenon is natural convection and occurs frequently in nature and is present in many industrial applications. The fluid movement is steady up to a critical Rayleigh number, above which vortices are formed along the hot and the cold walls. Further increase of temperature difference leads through oscillatory behaviour to turbulent natural convection [22]. The phenomenon is defined by the type of fluid, temperature difference and the layout of the enclosure.

In this work we will consider air as the working fluid, for which density ρ_0, viscosity ν_0 and diffusivity α_0 will be considered constant. The Prandtl number will be set to $Pr = \nu_0/\alpha_0 = 0.71$. Let the distance between the hot and cold walls be the width of the enclosure $\mathscr{W}$. We will nondimensionalize all quantities, velocity $\vec{v}$, vorticity $\vec{\omega} = \vec{\nabla} \times \vec{v}$, temperature T, time t, position vector $\vec{r}$ in the following manner:

$$\vec{v} \to \frac{\vec{v}}{v_0}, \quad \vec{g} \to \frac{\vec{g}}{g_0}, \quad \vec{r} \to \frac{\vec{r}}{\mathscr{W}}, \quad \vec{\omega} \to \frac{\vec{\omega}\mathscr{W}}{v_0},$$
$$t \to \frac{v_0 t}{\mathscr{W}}, \quad T \to \frac{T - T_0}{\Delta T}, \quad v_0 = \frac{\alpha_0}{\mathscr{W}}, \tag{1}$$

where $g_0 = 9.81\ m/s^2$, ΔT is the temperature difference between the hot and cold walls and $T_0 = (T_{\text{hot}} + T_{\text{cold}})/2$. The gravity force works in the negative z direction. The enclosure will be inclined for an angle ϑ from the gravity direction in such a way that the hot wall will be located above the cold wall. The enclosure will be $\mathscr{W}$ wide, $\mathscr{D}$ deep and $\mathscr{H}$ high. The computational domain extents are $(0,0,0) \times (1, \mathscr{D}/\mathscr{W}, \mathscr{H}/\mathscr{W})$. The coordinate system axes lie along the edges of the enclosure. With this, the gravity vector is related to the inclination angle by

$$\vec{g} = (-\sin\vartheta, 0, -\cos\vartheta). \tag{2}$$

The temperature $T = -0.5$ will be prescribed at $x = 0$ and $T = 0.5$ at $x = 1$. The other four walls are adiabatic, i.e. there is no temperature flux through them. Since we consider a closed enclosure, non-slip velocity boundary

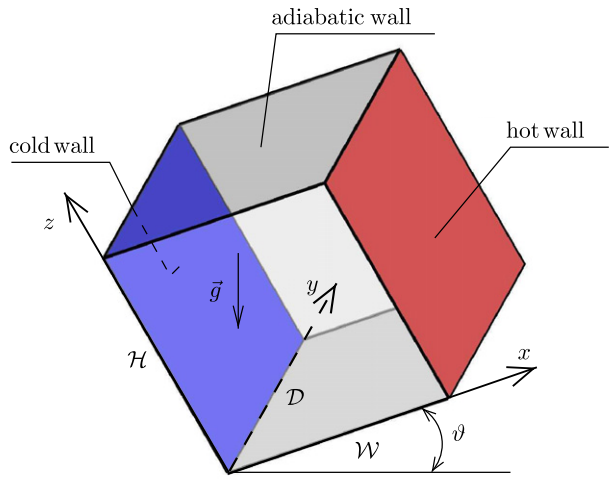

Fig. 1. Sketch of an inclined enclosure with width $\mathscr{W}$, depth $\mathscr{D}$ and height $\mathscr{H}$. Natural convection is induced by keeping two opposite walls at constant (hot and cold) temperatures, while the other four walls are presumed to be without temperature flux, i.e. adiabatic.

conditions $\vec{v} = 0$ are applied on all walls. The layout of the problem is shown in Fig. 1.

3. Governing equations

The velocity–vorticity formulation of Navier–Stokes equations consists of the kinematics equation and the vorticity transport equation. The kinematics equation is a vector elliptic partial differential equation of Poisson type and links the velocity and vorticity fields for every point in space and time. It is equivalent to the Biot–Savart law, which connects the electric current and magnetic field density. The same connection that links the electric current and magnetic field density links velocity and vorticity fields in fluid flow [23]. For an incompressible fluid it can be stated as

$$\nabla^2\vec{v} + \vec{\nabla} \times \vec{\omega} = 0, \tag{3}$$

where we must bear in mind, that both velocity and vorticity fields are divergence free.

The kinetic aspect of fluid movement is governed by the vorticity transport equation. Buoyancy is modelled within the Boussinesq approximation. Density variations with temperature $\rho(T) = \rho_0[1 - \beta_T(T - T_0])$ are considered only in the buoyancy term and defined by the thermal volume expansion coefficient β_T and the temperature difference. Using this assumptions we may write the vorticity transport equation as:

$$\frac{\partial\vec{\omega}}{\partial t} + (\vec{v}\cdot\vec{\nabla})\vec{\omega} = (\vec{\omega}\cdot\vec{\nabla})\vec{v} + Pr\nabla^2\vec{\omega} - PrRa\vec{\nabla}\times T\vec{g}, \tag{4}$$

with Rayleigh Ra number defined as:

$$Ra = \frac{g_0\beta_T\Delta T\mathscr{W}^3}{\nu_0\alpha_0}. \tag{5}$$

Eq. (4) equates the advective vorticity transport on the left hand side with the vortex twisting and stretching term, the diffusion term and the buoyancy term on the right hand side. We further assume that no internal energy sources are present in the fluid. We will not deal with high velocity flow of highly viscous fluid, hence we will neglect irreversible viscous dissipation. With this, the internal energy conservation law, written with temperature as the unknown variable, reads as:

$$\frac{\partial T}{\partial t} + (\vec{v}\cdot\vec{\nabla})T = \nabla^2 T. \tag{6}$$

The partial differential equations (3), (4) and (6) form a nonlinear system for the unknown velocity, vorticity and temperature fields. The problem is in a given domain uniquely defined by specifying the Prandtl and Rayleigh numbers.

4. Numerical method

We will apply a combination of subdomain BEM and single domain BEM for the solution of the governing equations. The Dirichlet and/or Neumann boundary conditions for velocity and temperature are given. They are used to obtain solutions of the kinematics equation (3) for domain velocity values and energy equation (6) for domain temperature values. The boundary conditions for vorticity, which are needed to solve the vorticity transport equation (4), are unknown. This is not entirely true, since we are dealing with an enclosure with non-slip velocity boundary conditions, we know, that $\omega_j = 0$ at walls where $x_j = \text{const}; x_j = x, y, z$. We will use the single domain BEM on the kinematics equation to obtain the remaining unknown boundary vorticity values. The outline of the algorithm is as follows:

- initialization, calculate integrals;
- begin nonlinear loop;
  - calculate boundary vorticity values by solving the kinematics equation (3) by single domain BEM,
  - calculate domain velocity values by solving the kinematics equation (3) by subdomain BEM,
  - solve the energy equation (6) using the new velocity field for domain temperature values by subdomain BEM,
  - solve vorticity transport equation (4) by subdomain BEM for domain vorticity values using the boundary values from the solution of the kinematics equation and new velocity and temperature fields,
  - check convergence – repeat steps in the nonlinear loop until convergence of all field functions is achieved,
- end nonlinear loop;
- output results.

4.1. Subdomain BEM

The subdomain BEM will be used to solve the vorticity transport equation for domain vorticity values, the energy

equation for domain temperature values and the kinematics equation for domain velocity values. In the following subsections we describe solution of each of the three equations.

4.1.1. Subdomain BEM solution of the vorticity transport equation

Let us consider a domain Ω with a position vector $\vec{r} \in \mathbb{R}^3$. The boundary of the domain is $\Gamma = \partial\Omega$. In this work we are simulating a natural convection phenomena up to $Ra \leqslant 10^5$. The flow field in this case is steady, thus we may write $\partial\vec{\omega}/\partial t = 0$. The boundary-domain integral form of the steady vorticity transport equation (4) is [24]

$$c(\vec{\theta})\vec{\omega}(\vec{\theta}) + \int_\Gamma \vec{\omega}\vec{\nabla}u^\star \cdot \vec{n}\,\mathrm{d}\Gamma = \int_\Gamma u^\star \vec{q}\,\mathrm{d}\Gamma + \frac{1}{Pr}\int_\Omega u^\star\{(\vec{v}\cdot\vec{\nabla})\vec{\omega} - (\vec{\omega}\cdot\vec{\nabla})\vec{v}\}\,\mathrm{d}\Omega + Ra\int_\Omega u^\star\vec{\nabla}\times T\vec{g}\,\mathrm{d}\Omega, \tag{7}$$

where $\vec{\theta}$ is the source or collocation point, $\vec{n}$ is a vector normal to the boundary, pointing out of the domain and $u^\star$ is the fundamental solution for the diffusion operator:

$$u^\star = \frac{1}{4\pi|\vec{\theta} - \vec{r}|}. \tag{8}$$

$c(\vec{\theta})$ is the geometric factor defined as $c(\vec{\theta}) = \alpha/4\pi$, where α is the inner angle with origin in $\vec{\theta}$. If $\vec{\theta}$ lies inside of the domain then $c(\vec{\theta}) = 1; c(\vec{\theta}) = 1/2$, if $\vec{\theta}$ lies on a smooth boundary. Vorticity on the boundary $\vec{\omega}(\vec{r})$ or vorticity flux on the boundary $\vec{q}(\vec{r}) = \vec{\nabla}\vec{\omega}(\vec{r})\cdot\vec{n}$ are prescribed as boundary conditions.

Both domain integrals on the right hand side of Eq. (7) include derivatives of the unknown field functions. In the following we will use algebraic relations to move the derivative from the unknown field function to the fundamental solution. Let us first write the first domain integral alone for jth component of vorticity only:

$$\frac{1}{Pr}\int_\Omega\{(\vec{v}\cdot\vec{\nabla})\omega_j - (\vec{\omega}\cdot\vec{\nabla})v_j\}u^\star\Omega. \tag{9}$$

Due to the solenoidality of the velocity and vorticity fields, we may use $(\vec{\omega}\cdot\vec{\nabla})v_j = \vec{\nabla}\cdot(\vec{\omega}v_j)$ and $(\vec{v}\cdot\vec{\nabla})\omega_j = \vec{\nabla}\cdot(\vec{v}\omega_j)$ to transform equation (9) into

$$\frac{1}{Pr}\int_\Omega\{\vec{\nabla}\cdot(\vec{v}\omega_j - \vec{\omega}v_j)\}u^\star\,\mathrm{d}\Omega. \tag{10}$$

In order to move the derivative towards the fundamental solution, the following algebraic relation $\vec{\nabla}\cdot\{u^*(\vec{v}\omega_j - \vec{\omega}v_j)\} = u^*\vec{\nabla}\cdot(\vec{v}\omega_j - \vec{\omega}v_j) + (\vec{v}\omega_j - \vec{\omega}v_j)\cdot\vec{\nabla}u^*$ is used to obtain two integrals

$$\frac{1}{Pr}\int_\Omega\vec{\nabla}\cdot\{u^*(\vec{v}\omega_j - \vec{\omega}v_j)\}d\Omega - \frac{1}{Pr}\int_\Omega(\vec{v}\omega_j - \vec{\omega}v_j)\cdot\vec{\nabla}u^\star\,\mathrm{d}\Omega. \tag{11}$$

The first integral may be converted to a boundary integral using a Gauss divergence clause. Thus, the final form of the first domain integral of Eq. (7) for jth vorticity component without derivatives of field functions may be stated as:

$$\frac{1}{Pr}\int_\Gamma\vec{n}\cdot\{u^*(\vec{v}\omega_j - \vec{\omega}v_j)\}\,\mathrm{d}\Gamma - \frac{1}{Pr}\int_\Omega(\vec{v}\omega_j - \vec{\omega}v_j)\cdot\vec{\nabla}u^*\,\mathrm{d}\Omega. \tag{12}$$

In order to remove the derivative of temperature from the second domain integral of Eq. (7), we make use of the following algebraic relation: $\vec{\nabla}\times(u^\star T\vec{g}) = u^\star\vec{\nabla}\times T\vec{g} + T\vec{\nabla}\times u^\star\vec{g}$, which gives

$$+Ra\int_\Omega\vec{\nabla}\times(u^\star T\vec{g})\,\mathrm{d}\Omega - Ra\int_\Omega T\vec{\nabla}\times u^\star\vec{g}\,\mathrm{d}\Omega. \tag{13}$$

With the aid of the Gauss clause we are able to transform the first domain integral of Eq. (13) into a boundary integral:

$$-Ra\int_\Gamma u^\star T\vec{g}\times\vec{n}\,\mathrm{d}\Gamma - Ra\int_\Omega T\vec{\nabla}\times u^\star\vec{g}\,\mathrm{d}\Omega, \tag{14}$$

yielding an expression without derivatives of the temperature field. Using expressions (12) and (14) instead of the domain integrals in Eq. (7), we may write the final integral form of the vorticity transport equation as:

$$c(\vec{\theta})\omega_j(\vec{\theta}) + \int_\Gamma\omega_j\vec{\nabla}u^*\cdot\vec{n}\,\mathrm{d}\Gamma = \int_\Gamma u^* q_j\,\mathrm{d}\Gamma + \frac{1}{Pr}\int_\Gamma\vec{n}\cdot\{u^*(\vec{v}\omega_j - \vec{\omega}v_j)\}\,\mathrm{d}\Gamma - \frac{1}{Pr}\int_\Omega(\vec{v}\omega_j - \vec{\omega}v_j)\cdot\vec{\nabla}u^*\,\mathrm{d}\Omega - Ra\int_\Gamma(u^\star T\vec{g}\times\vec{n})_j\,\mathrm{d}\Gamma - Ra\int_\Omega(T\vec{\nabla}\times u^\star\vec{g})_j\,\mathrm{d}\Omega. \tag{15}$$

In the subdomain BEM method we make a mesh of the entire domain Ω and name each mesh element a subdomain. Eq. (15) is written for each of the subdomains. In order to obtain a discrete version of (15) we use shape functions to interpolate field functions and flux across the boundary and inside of the subdomain. In this work we used hexahedral subdomains with 27 nodes, which enable continuous quadratic interpolation of field functions. The boundary of each hexahedron consists of six boundary elements. On each boundary element we interpolate the flux using discontinuous linear interpolation scheme with four nodes. By using discontinuous interpolation we avoid flux definition problems in corners and edges. A subdomain and one boundary element are sketched in Fig. 2. A function, e.g. temperature, is interpolated over a boundary elements as $T = \sum\varphi_i T_i$, inside each subdomain as $T = \sum\Phi_i T_i$, while flux is interpolated over boundary elements as $q = \sum\phi_i q_i$. The following integrals must be calculated:

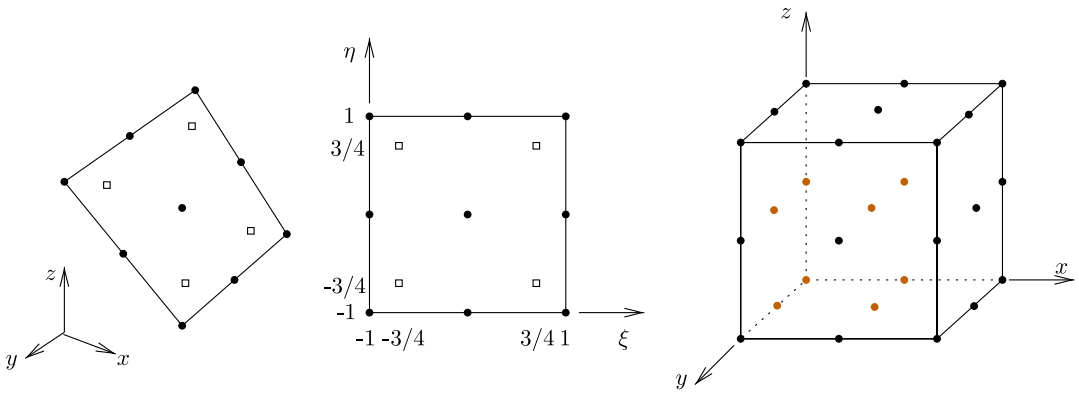

Fig. 2. A boundary element in $\mathbb{R}^3$ space (left) and in a local coordinate system (middle) with function (circles) and flux (squares) nodes. A hexahedral subdomain with function nodes is shown on the right.

$$[H] = \int_\Gamma \varphi_i \vec{\nabla} u^\star \cdot \vec{n}\, \mathrm{d}\Gamma, \quad [G] = \int_\Gamma \phi_i u^\star \, \mathrm{d}\Gamma, \tag{16}$$

$$[\vec{A}] = \int_\Gamma \varphi_i \vec{n} u^\star \, \mathrm{d}\Gamma, \quad [\vec{D}] = \int_\Omega \Phi_i \vec{\nabla} u^\star \, \mathrm{d}\Omega. \tag{17}$$

The square brackets denote integral matrices. Each source point location yields one row in these matrices. The number of columns is 26 for $[H]$ and $[\vec{A}]$ matrices, since there are 26 function nodes on the surface of each subdomain. The matrix $[G]$ has 24 columns, since there are 24 flux nodes on the surface of each subdomain. Matrices $[\vec{D}]$ have 27 columns since there are 27 nodes in each subdomain. In order to calculate the integrals, a Gaussian quadrature algorithm is used. The integrals are calculated in local coordinate system via weighted summation of up to 48 integration points per coordinate axis. Calculation of the free coefficient $c(\vec{\theta})$ is preformed indirectly. If we consider a rigid body movement, $u = 1$, $q = 0$, we see that the sum of all $[H]$ matrix elements for one source point must be equal to 0, thus we may use this fact to calculate $c(\vec{\theta})$. The calculated $c(\vec{\theta})$ are added to the diagonal terms of the $[H]$ matrix.

The source point is set to all function and flux node in each subdomain. That makes the number of rows of each matrix 51 times the number of subdomains. By letting curly brackets denote vectors of nodal values of field functions, we may write the discrete vorticity transport equation in component form as:

$$\begin{aligned}[H]\{\omega_x\} = {} & [G]\{q_x\} + \frac{1}{Pr}[A_y]\{v_y\omega_x - \omega_y v_x\} \\ & + \frac{1}{Pr}[A_z]\{v_z\omega_x - \omega_z v_x\} - \frac{1}{Pr}[D_y]\{v_y\omega_x - \omega_y v_x\} \\ & - \frac{1}{Pr}[D_z]\{v_z\omega_x - \omega_z v_x\} + Ra(g_z[A_y]\{T\} \\ & - g_y[A_z]\{T\} - g_z[D_y]\{T\} + g_y[D_z]\{T\}),\end{aligned} \tag{18}$$

$$\begin{aligned}[H]\{\omega_y\} = {} & [G]\{q_y\} + \frac{1}{Pr}[A_x]\{v_x\omega_y - \omega_x v_y\} \\ & + \frac{1}{Pr}[A_z]\{v_z\omega_y - \omega_z v_y\} - \frac{1}{Pr}[D_x]\{v_x\omega_y - \omega_x v_y\} \\ & - \frac{1}{Pr}[D_z]\{v_z\omega_y - \omega_z v_y\} + Ra(g_x[A_z]\{T\} \\ & - g_z[A_x]\{T\} + g_z[D_x]\{T\} - g_x[D_z]\{T\}),\end{aligned} \tag{19}$$

$$\begin{aligned}[H]\{\omega_z\} = {} & [G]\{q_z\} + \frac{1}{Pr}[A_x]\{v_x\omega_z - \omega_x v_z\} \\ & + \frac{1}{Pr}[A_y]\{v_y\omega_z - \omega_y v_z\} - \frac{1}{Pr}[D_x]\{v_x\omega_z - \omega_x v_z\} \\ & - \frac{1}{Pr}[D_y]\{v_y\omega_z - \omega_y v_z\} + Ra(g_y[A_x]\{T\} \\ & - g_x[A_y]\{T\} - g_y[D_x]\{T\} + g_x[D_y]\{T\}).\end{aligned} \tag{20}$$

Since neighbouring subdomains share nodes, the systems of linear equations (18)–(20) are over-determined. After taking into account the boundary conditions, we solve them using a least squares solver [25]. All integrals depend only on the shape of subdomains and as such may be calculated only once, prior to the start of the nonlinear iterative process.

4.1.2. Subdomain BEM solution of the energy equation

The energy equation (6) is a diffusion convection partial differential equation exactly like the vorticity transport equation without the vortex twisting and stretching and buoyancy terms. The solution of (6) is thus obtained in the same manner than the solution of the vorticity transfer equation. The same integral matrices are required. The discrete counterpart of the energy equation (6) is

$$\begin{aligned}[H]\{T\} = {} & [G]\{q_T\} + [A_x]\{v_x T\} + [A_y]\{v_y T\} + [A_z]\{v_z T\} \\ & - [D_x]\{v_x T\} - [D_y]\{v_y T\} - [D_z]\{v_z T\},\end{aligned} \tag{21}$$

where $\{q_T\}$ is a nodal vector of temperature flux. Boundary conditions are either known temperature or temperature flux on the boundary. We set up the system matrix from $[H]$ and $[G]$ matrices accordingly. The system matrix is sparse and as such it is stored efficiently in a compressed row storage format. The system is solved in a least squares manner [25].

4.1.3. Subdomain BEM solution of the kinematics equation

The integral form of the kinematics equation without derivatives of the velocity and vorticity fields takes the following form (for derivation, see Ravnik et al. [22] Eqs. (19)–(24)):

$$c(\vec{\theta})\vec{v}(\vec{\theta}) + \int_\Gamma \vec{v}\vec{\nabla}u^\star \cdot \vec{n}\,\mathrm{d}\Gamma = \int_\Gamma \vec{v}\times(\vec{n}\times\vec{\nabla})u^\star\,\mathrm{d}\Gamma + \int_\Omega(\vec{\omega}\times\vec{\nabla}u^\star)\,\mathrm{d}\Omega. \quad (22)$$

The boundary integral on the left hand side are stored in the $[H]$ matrix, the domain integrals on the right hand side are the $[\vec{D}]$ matrices. We define the boundary integral on the right hand side as $[\vec{H}^{\mathrm{t}}]$ integrals in the following manner:

$$[\vec{H}^{\mathrm{t}}] = \int_\Gamma \varphi_i(\vec{n}\times\vec{\nabla})u^\star\,\mathrm{d}\Gamma. \quad (23)$$

Since there are no fluxes in the equation, the source point is set to function nodes only. The discrete kinematics equation written in component wise form is

$$[H]\{v_x\} = [H_z^{\mathrm{t}}]\{v_y\} - [H_y^{\mathrm{t}}]\{v_z\} + [D_z]\{\omega_y\} - [D_y]\{\omega_z\}, \quad (24)$$

$$[H]\{v_y\} = [H_x^{\mathrm{t}}]\{v_z\} - [H_z^{\mathrm{t}}]\{v_x\} - [D_z]\{\omega_x\} + [D_x]\{\omega_z\}, \quad (25)$$

$$[H]\{v_z\} = [H_y^{\mathrm{t}}]\{v_x\} - [H_x^{\mathrm{t}}]\{v_y\} + [D_y]\{\omega_x\} - [D_x]\{\omega_y\}. \quad (26)$$

The kinematics equation takes the same form for fluid flow problems and for coupled fluid flow – heat transfer problems. Thus, the solution procedure employed here is the same as it was used in an algorithm for the solution of 3D laminar viscous flow [17].

4.2. Single domain BEM

In order to use the kinematics equation to obtain boundary vorticity values, we must rewrite Eq. (22) in a tangential form by multiplying the system with a normal in the source point $\vec{n}(\vec{\theta})$:

$$c(\vec{\theta})\vec{n}(\vec{\theta})\times\vec{v}(\vec{\theta}) + \vec{n}(\vec{\theta})\times\int_\Gamma \vec{v}\vec{\nabla}u^\star\cdot\vec{n}\,\mathrm{d}\Gamma = \vec{n}(\vec{\theta})\times\int_\Gamma \vec{v}\times(\vec{n}\times\vec{\nabla})u^\star\,\mathrm{d}\Gamma + \vec{n}(\vec{\theta})\times\int_\Omega(\vec{\omega}\times\vec{\nabla}u^\star)\,\mathrm{d}\Omega. \quad (27)$$

This approach has been proposed by Škerget and used in 2D by Škerget et al. [16] and in 3D by Žunič et al. [26] and Ravnik et al. [17]. In order to write a linear system of equations for the unknown boundary vorticity values, we set the source point into every boundary node of the whole computational domain. This yields a full system matrix with number of boundary nodes rows and columns. It is solved using a LU decomposition method. Since this equation and its solution are the same for coupled and uncoupled flow and heat transfer problems, please examine the references above for a complete detailed description of the single domain BEM procedure.

5. Results

We studied the natural convection phenomena in two type of enclosures: a cube with $\mathscr{H} = \mathscr{D} = \mathscr{W}$ and a parallelepiped with $\mathscr{H} = 2\mathscr{W}$ and $\mathscr{D} = \mathscr{W}$ (Fig. 1). Both enclosures were inclined for angles between $\vartheta = 0^\circ$ and $\vartheta = 60^\circ$ and subjected to temperature differences corresponding to Rayleigh numbers ranging from $Ra = 10^3$ to $Ra = 10^5$.

Three meshes were used in the analysis. The very coarse mesh with 8^3 subdomains and 17^3 nodes, the coarse mesh with 10^3 subdomains and 21^3 nodes and the fine mesh with 12^3 subdomains and 25^3 nodes. Subdomains were concentrated towards the hot and the cold walls. The stopping criteria for the least squares solver was 10^{-7}. The nonlinear loop continued until the RMS difference between iterations of all field functions was less than 10^{-6}. For a cubic enclosure about 100 iterations were necessary to achieve the stopping criteria using an under-relaxation of vorticity and temperature values of 0.1. The same is valid to the $\mathscr{H} = 2\mathscr{W}$ enclosure for $Ra \leqslant 10^4$, while under-relaxation of 0.01 was used in the $Ra = 10^5$ case requiring about a 1000 iterations. By increasing the inclination angle the number of the necessary iterations decreased.

In order to validate our numerical algorithm, we compared our results with the results of Tric et al. [7] and Lo et al. [8]. Tric et al. [7] studied natural convection in a cubic enclosure without inclination, $\vartheta = 0^\circ$, using a pseudo-spectra Chebyshev algorithm based on the projection–diffusion method with spatial resolution supplied by polynomial expansions. Lo et al. [8] also studied a cubic enclosure under five different inclinations $\vartheta = 0^\circ, 15^\circ, 30^\circ, 45^\circ, 60^\circ$. They used a differential quadrature method to solve the velocity–vorticity formulation of Navier–Stokes equations employing higher order polynomials to approximate differential operators.

Both studies provided their results in terms of the Nusselt number Nu. The Nusselt number is a nondimensional quantity defined as the integral of the temperature flux through a wall divided by the area of the wall. In our geometry this may be written as

$$Nu = \frac{\mathscr{W}^2}{\mathscr{H}\mathscr{D}}\int_0^{\mathscr{D}/\mathscr{W}}\int_0^{\mathscr{H}/\mathscr{W}} \frac{\partial T}{\partial x}\,\mathrm{d}z\,\mathrm{d}y. \quad (28)$$

Table 1 presents Nusselt number values for the cubic enclosure without inclination. Results obtained with our method on three meshes are compared with benchmark results. With the increasing mesh density our results converge nicely to the benchmark making the 25^3 mesh results in good agreement with the benchmark.

Nusselt number estimation for an inclined cubic enclosure are presented in Table 2. Again we can confirm that

Table 1
Natural convection in a cubic enclosure without inclination, $\vartheta = 0$

Ra	[8]	[7]	17^3	21^3	25^3
10^3	1.0710	1.0700	1.0716	1.0710	1.0713
10^4	2.0537	2.0542	2.0664	2.0627	2.0591
10^5	4.3329	4.3371	4.3893	4.3768	4.3570

Present Nusselt number values are compared with the benchmark results of Lo et al. [8] and Tric et al. [7].

Table 2
Natural convection in a cubic enclosure under inclination ϑ

ϑ	[8]	17^3	25^3	[8]	17^3	25^3	[8]	17^3	25^3
	$Ra = 10^3$			$Ra = 10^4$			$Ra = 10^5$		
15°	1.0590	1.0595	1.0592	1.8425	1.8525	1.8464	3.7731	3.8149	3.7881
30°	1.0432	1.0435	1.0433	1.5894	1.5955	1.5916	2.9014	2.9227	2.9071
45°	1.0268	1.0269	1.0268	1.3434	1.3460	1.3443	1.9791	1.9821	1.9782
60°	1.0127	1.0128	1.0127	1.1524	1.1531	1.1526	1.3623	1.3587	1.3600

Present Nusselt number values are compared with the benchmark results of Lo et al. [8].

the results obtained on the fine mesh are in good agreement with the reference for all inclination angles and Rayleigh number values.

Finally, we present the Nusselt number values for natural convection in an inclined $\mathscr{H}/\mathscr{W} = 2$ enclosure. Table 3 presents the values for $\vartheta = 0°, 15°, 30°, 45°$ and $60°$ and $10^3 \leqslant Ra \leqslant 10^5$.

Comparison of Nusselt number values for both types of enclosures is presented graphically in Fig. 3. In both cases we observe an increase of the Nusselt number with increasing Rayleigh number and a decrease of the Nusselt number with increasing inclination angle. The $\mathscr{H}/\mathscr{W} = 2$ enclosure yields higher Nusselt values than the cubic enclosure.

Fig. 4 presents the temperature profiles. We may observe that the temperature gradients are highest close to the hot and the cold walls in the $\vartheta = 0°$ case. As the enclosure is inclined the temperature gradients decrease. As a result the heat transfer through the walls is lower and consequently the Nusselt number values as also lower. Fig. 4 displays profiles only up to $\vartheta = 30°$. At larger inclination angles the Nusselt number is close to unity and thus all profiles are very close to the linear profile. Fig. 5 displays temperature contours in the $y = 0.5$ plane at $Ra = 10^5$ for different inclination angles. We see that regardless of the inclination angle or the shape of the enclosure the temperature is stratified, i.e. we observe layers of air with equal temperature perpendicular to the direction of gravity. We noticed the same effect when observing the temperature fields at $Ra = 10^3$ and $Ra = 10^4$. The stratification was observed in the central parts of the enclosures by other authors as well [10,22]).

Table 3
Natural convection in a $\mathscr{H}/\mathscr{W} = 2$ enclosure

ϑ	$Ra = 10^3$	$Ra = 10^4$	$Ra = 10^5$
0°	1.111	2.163	4.177
15°	1.096	2.029	3.892
30°	1.073	1.839	3.430
45°	1.047	1.594	2.774
60°	1.023	1.317	1.915

The Nusselt number values representing the heat flux through walls are shown for different inclination angles and Rayleigh numbers. Simulations were preformed on a mesh with 25^3 nodes.

The maximum difference between present Nusselt number values (Tables 1 and 2) and benchmark results is for all Rayleigh number values observed at $\vartheta = 0°$. This can be explained considering the fact that as the inclination angle increases the temperature gradient at the walls decreases. The gradients are steepest and the flow field is most complex at $\vartheta = 0°$. Consequently, it is more difficult to simulate the $\vartheta = 0°$ flow field, than flows at other inclination angles.

By observing the velocity profiles in Fig. 6 we observe that the fluid moves fastest along the hot and the cold walls. Considerable velocity is found along the top and bottom walls as well, making the primary vortex in the x–z plane. Examining the flow structure in the enclosures, we observe that the flow field is not far from being 2D. The

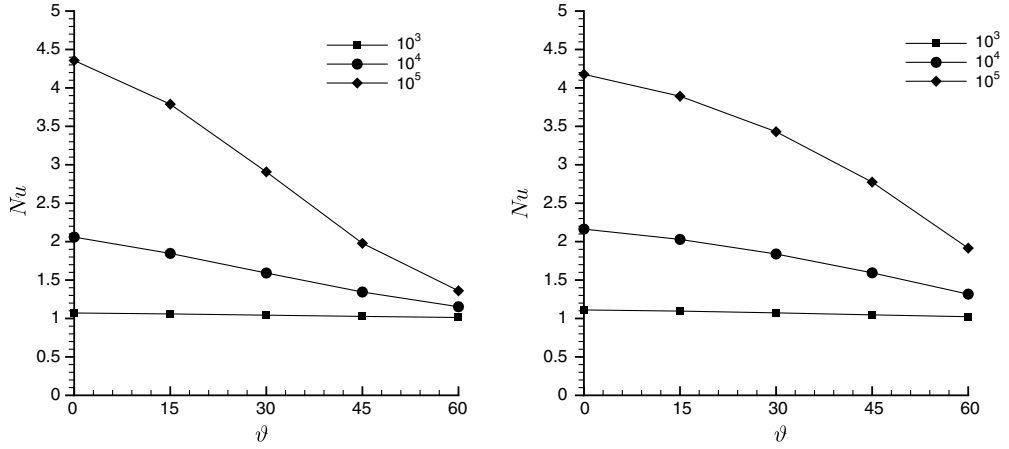

Fig. 3. Dependence of the Nusselt number on the inclination angle ϑ; left cubic enclosure, right a $\mathscr{H}/\mathscr{W} = 2$ enclosure.

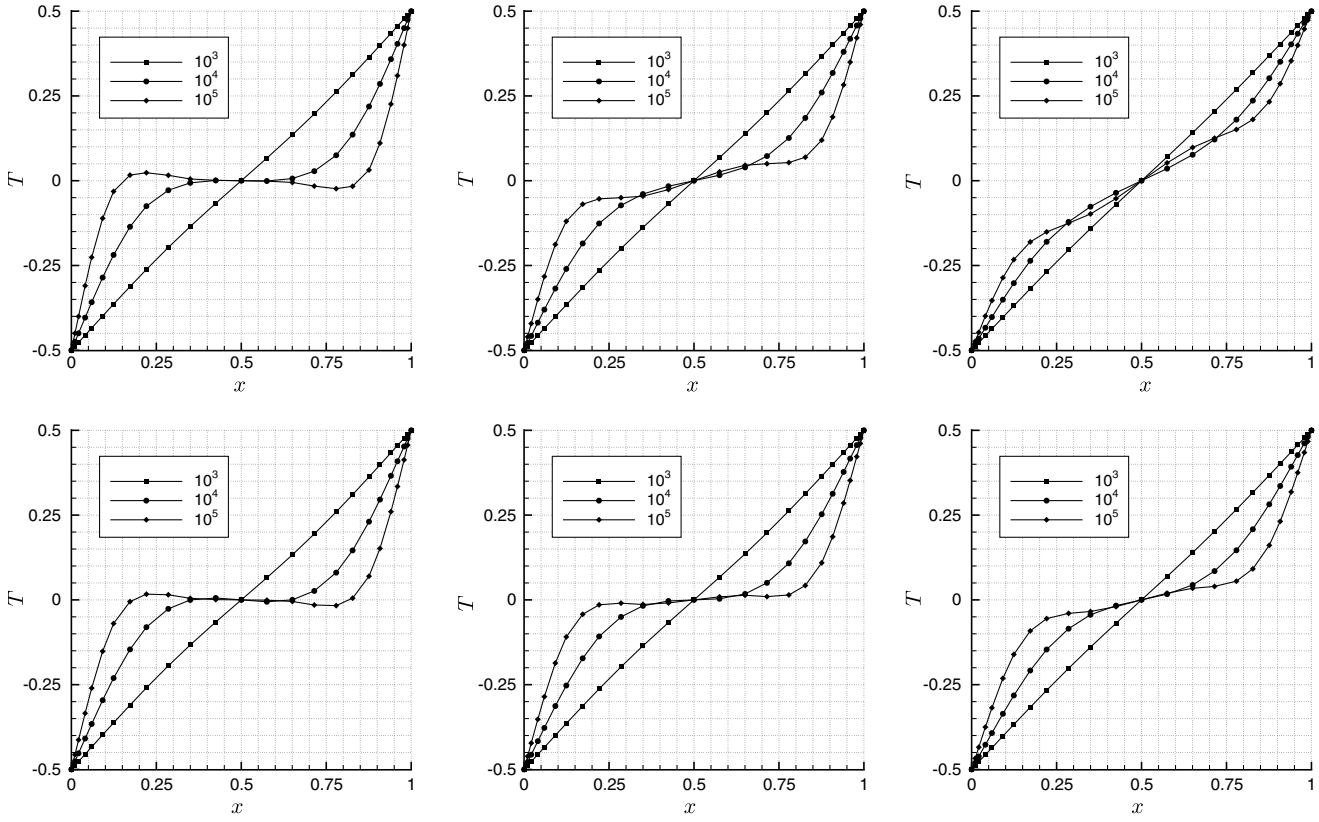

Fig. 4. Comparison of temperature profiles for the three Rayleigh number values, $y = 0.5$, $z = 0.5$, $\vartheta = 0^\circ$ (left), $\vartheta = 15^\circ$ (middle) and $\vartheta = 30^\circ$ (right). Top row: cubic enclosure, bottom row $\mathscr{H}/\mathscr{W} = 2$ enclosure.

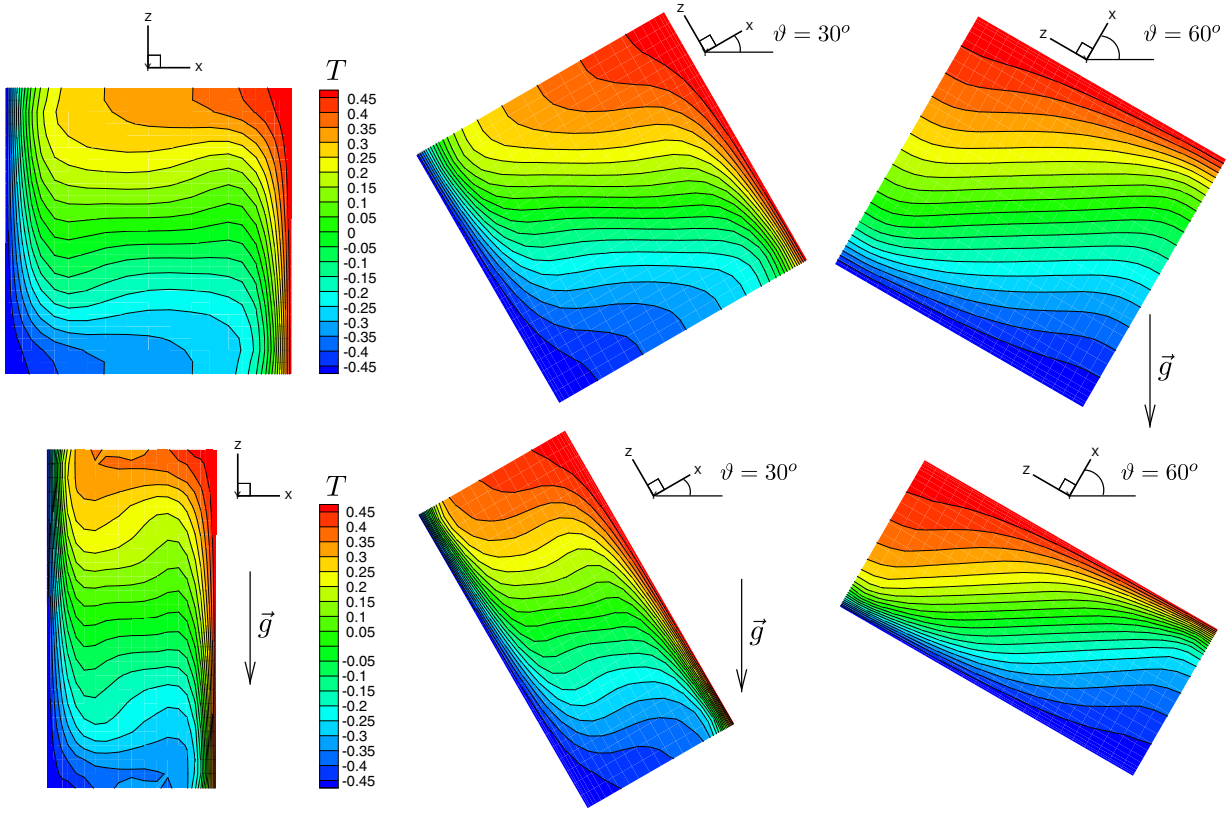

Fig. 5. Temperature contour plots on the $y = 0.5$ plane for Rayleigh number $Ra = 10^5$; $\vartheta = 0^\circ$ (left), $\vartheta = 15^\circ$ (middle) and $\vartheta = 30^\circ$ (right). Top row: cubic enclosure; bottom row: $\mathscr{H}/\mathscr{W} = 2$ enclosure. Gravity points downward in all cases.

fluid predominantly moves in the x–z plane. In order to show the 3D nature of the phenomena, we plotted iso-surfaces of y velocity component in Fig. 7. Although the extent of movement perpendicular to the x–z plane is small, it can be found in the corners of the enclosures. The fact that the 2D approximation of the natural convection in an enclosure is quite good in this Rayleigh number range can be confirmed by comparing the Nusselt number values. A 2D solution of natural convection of air in a square enclosure [1,11]) yield $Nu = 1.118$ for $Ra = 10^3$,

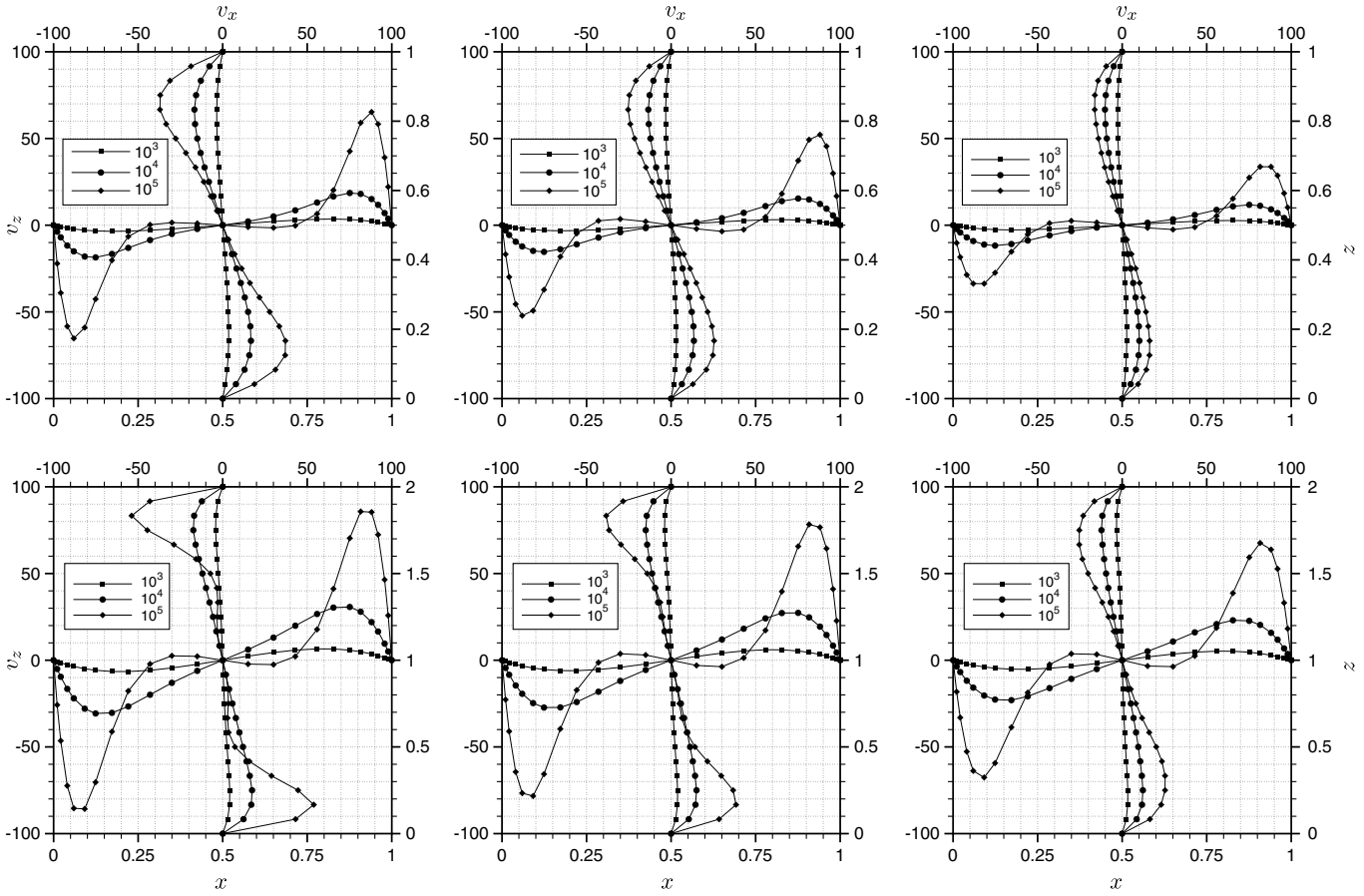

Fig. 6. Comparison of velocity profiles for the three Rayleigh number values; $v_x(0.5, 0.5, z), v_z(x, 0.5, 0.5); \vartheta = 0°$ (left), $\vartheta = 15°$ (middle) and $\vartheta = 30°$ (right). Top row: cubic enclosure; bottom row: $\mathscr{H}/\mathscr{W} = 2$ enclosure.

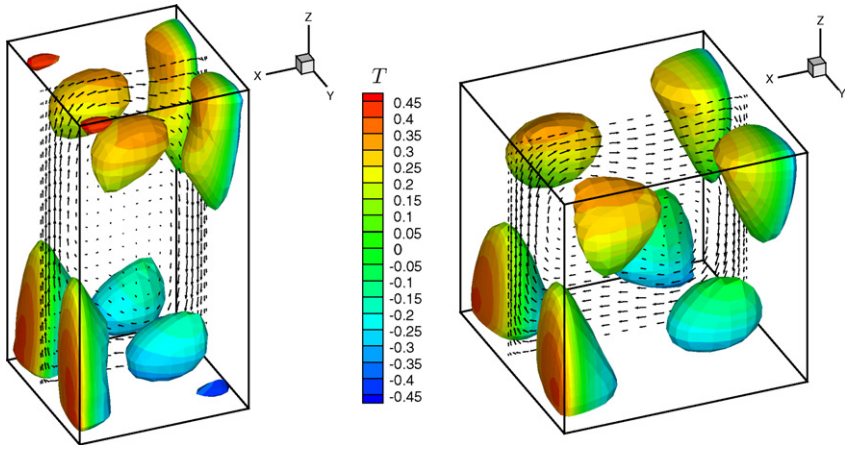

Fig. 7. Iso-surfaces of an absolute value of velocity component $|v_y| = 3$ shown along with velocity vectors in $y = 0.5$ plane for cubic enclosure (right) and $\mathscr{H}/\mathscr{W} = 2$ enclosure (left); $Ra = 10^5$, $\vartheta = 0°$. The iso-surfaces are coloured with temperature contours.

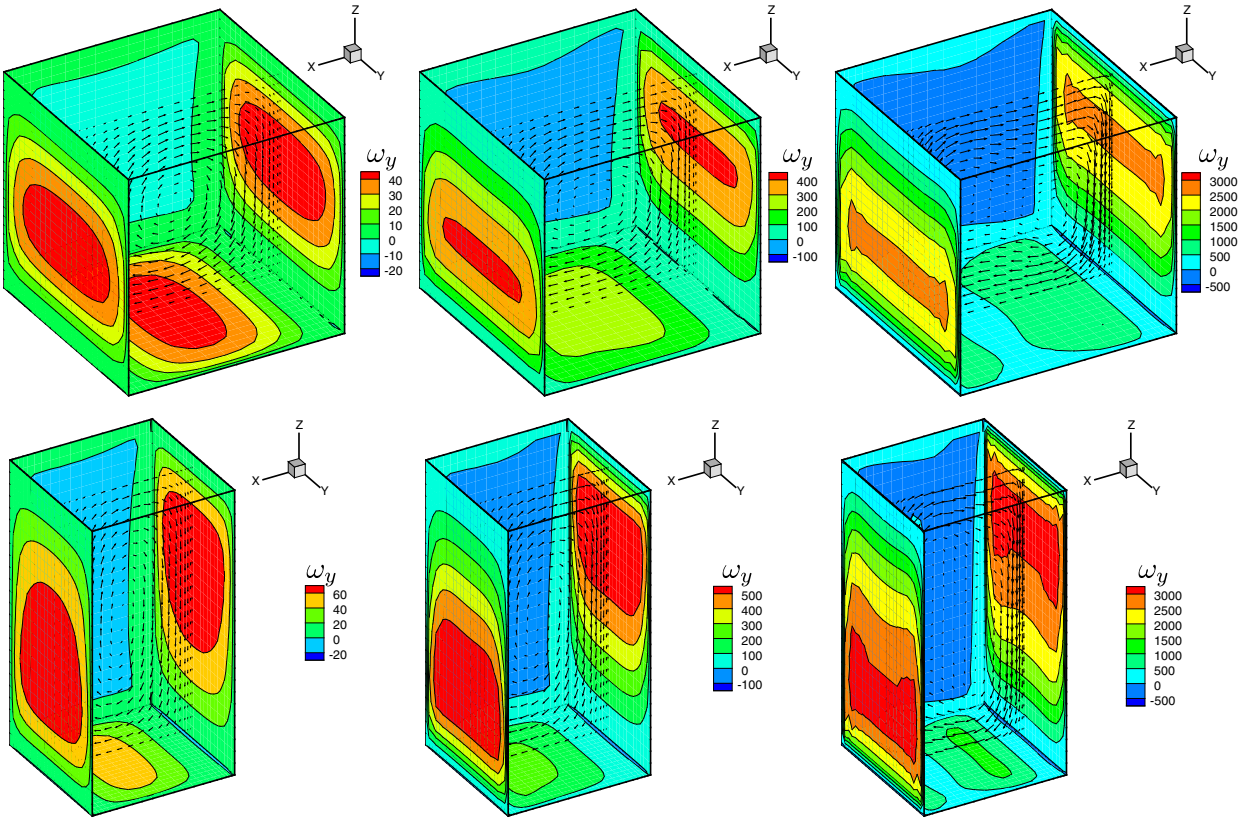

Fig. 8. Contours of the y component of vorticity, ω_y, for $Ra = 10^3$ (left), $Ra = 10^4$ (middle) and $Ra = 10^5$ (right); $\vartheta = 0°$. To illustrate the flow field, the velocity vectors on the $y = 0.5$ plane are shown as well.

$Nu = 2.243$ for $Ra = 10^4$ and $Nu = 4.519$ for $Ra = 10^5$, which are all quite close (within 8%) to the values obtained by the present 3D solution (Table 1). A 2D simulation predicts higher Nusselt number values than the full 3D simulation. Salat et al. [27] confirmed that 2D and 3D simulation give the same general flow structure even when modelling turbulent natural convection at high Rayleigh number values by studying experimental data, 2D LES, 2D DNS and 3D LES computations.

Fig. 8 shows the y vorticity component contours along the walls of the enclosures. We can see that the vorticity values grow rapidly with the increasing of the Rayleigh number. The largest vorticity values may be found at the bottom of the hot wall and at the top of the cold wall, where velocity gradients are highest. Comparing the cubic and $\mathscr{H}/\mathscr{W} = 2$ enclosures we observe that the high vorticity areas take up a larger portion of the wall in the $\mathscr{H}/\mathscr{W} = 2$ enclosure. Also, the vorticity values are higher in the $\mathscr{H}/\mathscr{W} = 2$ enclosure than in the cubic. This is due to the fact that the fluid is able to accelerate along a longer wall in the case of $\mathscr{H}/\mathscr{W} = 2$ enclosure and as such produces higher velocity gradients.

6. Conclusions

We presented a method for solving coupled laminar viscous flow and heat transfer problems. The algorithm solves the velocity–vorticity formulation of Navier–Stokes equations. The boundary vorticity values are obtained by the single domain BEM solution of the kinematics equation. The solution of the vorticity equation for domain vorticity values, the energy equation for domain temperature values and the kinematics equation for domain velocity values are obtained by subdomain BEM.

The method was used to simulate natural convection phenomena in inclined parallelepipedal enclosures. The method was validated by comparing Nusselt number values for $Ra = 10^3$ to $Ra = 10^5$ with benchmark results for an inclined cubic enclosure. In addition we presented temperature fields, velocity profiles and Nusselt number values for an enclosure with height to width ratio $\mathscr{H}/\mathscr{W} = 2$.

By studying the temperature field in the enclosure we observed, that in the central part the temperature field is stratified. The layers of constant temperature are set perpendicularly to the gravity direction regardless of the inclination angle as long as the hot wall lies above the cold wall. The velocity flow fields show that the flow is predominantly moving in a single vortex, up along the hot wall and down along the cold wall. The 3D nature of the flow may be observed in the corners of the enclosures. We have confirmed that the 2D approximation of the flow field is quite good. The 2D calculated Nusselt number values are quite close (within 8%) of the Nusselt number values obtained with a 3D simulation.

Comparing the cubic and $\mathscr{H}/\mathscr{W} = 2$ enclosures we established that the Nusselt number values are higher in the case of $\mathscr{H}/\mathscr{W} = 2$ enclosure. Moreover, comparison of temperature profiles, velocity vectors and vorticity values showed that higher values and steeper gradients may be found in the $\mathscr{H}/\mathscr{W} = 2$ enclosure.

In future we whish to expand our numerical method for simulation of turbulent natural convection at high Rayleigh numbers using velocity–vorticity formulation of LES.

References

[1] G.D.V. Davies, Natural convection of air in a square cavity: a bench mark numerical solution, Int. J. Numer. Meth. Fluid 3 (1983) 249–264.

[2] J. Vierendeels, B. Merci, E. Dick, Numerical study of the natural convection heat transfer with large temperature differences, Int. J. Num. Meth. Heat Fluid Flow 11 (2001) 329–341.

[3] J. Vierendeels, B. Merci, E. Dick, A multigrid method for natural convective heat transfer with large temperature differences, Int. J. Comput. Appl. Math. 168 (2004) 509–517.

[4] L. Škerget, N. Samec, BEM for the two-dimensional plane compressible fluid dynamics, Eng. Anal. Bound. Elem. 29 (2005) 41–57.

[5] C. Weisman, L. Calsyn, C. Dubois, P.L. Quéré, Sur la nature de la transition a l'instationare d'un ecoulement de convection naturelle en cavite differentiellement chauffee a grands ecarts de temperature, Comptes rendus de l'academie des sciences Serie II b, Mecanique (2001) 343–350.

[6] M.S. Ingber, A vorticity method for the solution of natural convection flows in enclosures, Int. J. Num. Meth. Heat Fluid Flow 13 (2003) 655–671.

[7] E. Tric, G. Labrosse, M. Betrouni, A first incursion into the 3D structure of natural convection of air in a differentially heated cubic cavity, from accurate numerical simulations, Int. J. Heat Mass Transfer 43 (2000) 4034–4056.

[8] D. Lo, D. Young, K. Murugesan, C. Tsai, M. Gou, Velocity–vorticity formulation for 3D natural convection in an inclined cavity by DQ method, Int. J. Heat Mass Transfer 50 (2007) 479–491.

[9] K.J. Hsieh, F.S. Lien, Numerical modelling of buoyancy-driven turbulent flows in enclosures, Int. J. Heat Fluid Flow 25 (4) (2004) 659–670.

[10] S. Xin, P.L. Quéré, Direct numerical simulations of two-dimensional chaotic natural convection in a differentially heated cavity of aspect ratio 4, J. Fluid Mech. 304 (1995) 87–118.

[11] J. Ravnik, L. Škerget, M. Hriberšek, The wavelet transform for BEM computational fluid dynamics, Eng. Anal. Bound. Elem. 28 (2004) 1303–1314.

[12] S.H. Peng, L. Davidson, Large eddy simulation for turbulent buoyant flow in a confined cavity, Int. J. Heat Fluid Flow 22 (2001) 323–331.

[13] O. Daube, Resolution of the 2D Navier–Stokes equations in velocity–vorticity form by means of an influence matrix technique, J. Comput. Phys. 103 (1992) 402–414.

[14] K.L. Wong, A.J. Baker, A 3D incompressible Navier–Stokes velocity–vorticity weak form finite element algorithm, Int. J. Num. Meth. Fluid 38 (2002) 99–123.

[15] C.H. Liu, Numerical solution of three-dimensional Navier Stokes equations by a velocity–vorticity method, Int. J. Numer. Meth. Fluid 35 (2001) 533–557.

[16] L. Škerget, M. Hriberšek, Z. Žunič, Natural convection flows in complex cavities by BEM, Int. J. Num. Meth. Heat Fluid Flow 13 (2003) 720–735.

[17] J. Ravnik, L. Škerget, Z. Žunič, Combined single domain and subdomain BEM for 3D laminar viscous flow, Eng. Anal. Bound. Elem., submitted for publication.

[18] V. Popov, H. Power, L. Škerget (Eds.), Domain Decomposition Techniques for Boundary Elements: Applications to fluid flow, WIT Press, 2007.

[19] M. Bebendorf, Approximation of boundary element matrices, Numer. Math 86 (2000) 565–589.

[20] B. Jumarhon, S. Amini, K. Chen, On the boundary element dual reciprocity method, Eng. Anal. Bound. Elem. 20 (1997) 205–211.

[21] K. Epplera, H. Harbrecht, Fast wavelet BEM for 3D electromagnetic shaping, Appl. Numer. Math. 54 (2005) 537–554.

[22] J. Ravnik, L. Škerget, M. Hriberšek, 2D velocity vorticity based LES for the solution of natural convection in a differentially heated enclosure by wavelet transform based BEM and FEM, Eng. Anal. Bound. Elem. 30 (2006) 671–686.

[23] T. Lundgren, P. Koumoutsakos, On the generation of vorticity at a free surface, J. Fluid Mech. 382 (1999) 351–366.

[24] L.C. Wrobel, The Boundary Element Method, John Willey & Sons, Ltd., 2002.

[25] C.C. Paige, M.A. Saunders, LSQR: an algorithm for sparse linear equations and sparse least squares, ACM Trans. Math. Software 8 (1982) 43–71.

[26] Z. Žunič, M. Hriberšek, L. Škerget, J. Ravnik, 3-D boundary element-finite element method for velocity–vorticity formulation of the Navier–Stokes equations, Eng. Anal. Bound. Elem. 31 (2007) 259–266.

[27] J. Salat, S. Xin, P. Joubert, A. Sergent, F. Penot, P.L. Quéré, Experimental and numerical investigation of turbulent natural convection in a large air-filled cavity, Int. J. Heat Fluid Flow 25 (2004) 824–832.